Measurement-Based Characterization of LOS and NLOS Drone-to-Ground Channels

Yan Shi, Rita Enami, John Wensowitch, and Joseph Camp

Department of Electrical Engineering, Southern Methodist University

Abstract— The last few years have seen a rapid growth in unmanned aerial vehicle (UAV) based innovations and technologies, particularly for smaller drones. The rapid response to natural disasters, high data rate access in public safety situations, and the robustness of long-haul communication relays are highly dependent on airborne communication networks. A more precise channel characterization of air-to-ground links is imperative to establish these drone-based communication networks. However, there have been very limited efforts to understand the unique propagation channels encountered in drone-based communications, especially for wideband beamforming systems. In this paper, we perform a measurement-driven study to characterize air-to-ground wireless channels between UAV platforms and terrestrial users in practical Line of Sight (LOS) and Non Line of Sight (NLOS) scenarios across a wide range of carrier frequencies, including cellular (900 MHz and 1800 MHz), and WiFi (5 GHz) frequency bands. Furthermore, we investigate the feasibility of drone-based beamforming using IEEE 802.11-like signaling. We find that the drone-to-ground path loss differences are frequency dependent and closely related to drone altitude. The drone-based beamforming system can improve throughput significantly over IEEE 802.11 SISO schemes with select carrier frequencies in both LOS and NLOS scenarios up to 73.6% and 120.1%, respectively. Since our study spans many critical frequency bands, these results serve as a fundamental step towards understanding drone-to-ground communications and impact of beamforming-based applications in future aerial networks.

Index Terms—Drone-to-ground Channel, Drone, Beamforming

I. INTRODUCTION

Drones are greatly impacting dozens of industries throughout the world with almost three million UAVs expected to be manufactured in 2017 [1]. Improvements to drone-based communications are critical for better radio propagation conditions, controllability, automation, and positioning in dangerous or hard-to-access regions for such applications as search and rescue, reconnaissance, and disaster recovery [2], [3]. Hence, the future development of airborne infrastructures necessitates precise channel characterization due to increasing interests in drone-based systems and their resulting data services. However, the following challenges exist in the deployment of drone-based communication systems: (*i.*) high levels of channel fluctuations caused by hovering and flying the aircraft, (*ii.*) limited coverage range of omni-directional antenna patterns at high altitudes, and (*iii.*) large power consumption introduced by both drone flight and wireless Internet connectivity [3]–[5].

While many works have evaluated air-to-ground radio channels, they largely use simplifying assumptions in a simulated environment [6]–[12] or evaluate single-antenna designs at a single frequency band in a single type of environment [3], [13]–[15]. In this work, we conduct a measurement campaign

(a) Measurement Scenarios   (b) Experiment Setup
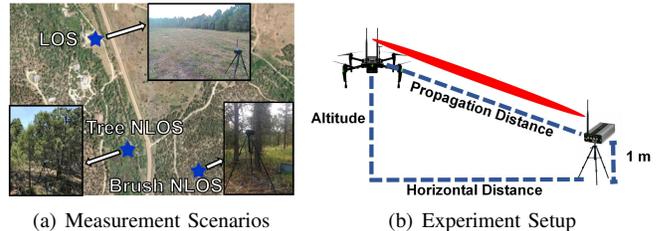
Fig. 1. Measurement Scenario for both LOS and NLOS Environments.

to study drone-to-ground channels across three environment types and a wide range of carrier frequencies (900 MHz, 1800 MHz, and 5 GHz) to consider propagation effects and system-level throughput of both Single Input Single Output (SISO) and beamforming-based communications. Specifically, we have performed month-long in-field measurements to investigate wideband signal propagation at one visual LOS location and two visual NLOS locations with two different vegetation-rich types, including a densely-treed environment and a brush environment, as shown by an aerial map in Fig. 1(a). To do so, we have mounted a Universal Software Radio Peripheral (USRP) platform (a battery-powered MIMO Ettus E312) on an off-the-shelf drone (a DJI Matrice 100 with 1 kg load capability) using 3-D printing. We have also developed an IEEE 802.11-like transmission framework on commercial drones that investigates the feasibility of air-to-ground beamforming systems (see Fig. 1(b)). We characterize the air-to-ground links by analyzing the dominant propagation parameters (*e.g.*, the path loss and shadowing standard deviation) and measuring the in-flight throughput achieved via our channel feedback approach for drone-based beamforming.

The main contributions of this paper are as follows:

- We build a drone-based beamforming system by securing a software defined radio platform on a drone via 3D printing and design an IEEE 802.11-like signaling mechanism to feedback channel state information (CSI) for both wideband and beamformed transmissions.
- We characterize three practical air-to-ground wireless channels (LOS, tree-based NLOS, and brush-based NLOS) at various drone heights and horizontal distances to the terrestrial-based receiver for three commonly-used frequency bands (900 MHz, 1800 MHz, and 5 GHz). We observe a peculiar effect where the metal drone body is a major factor in propagation, leading to high path loss at short horizontal distances when the drone is hovering at relatively higher altitude. We also find that the shadowing effect increases as the drone altitude increases, and NLOS can double the shadowing effect of a LOS area.

- We quantify the system-level throughput across these three in-field environments and frequency bands for both SISO and beamformed transmissions using our 802.11-like signaling mechanism. In particular, we observe beamforming gains of up to 73.6% and 120.1% in LOS and NLOS environments, respectively.

The rest of the paper is organized as follows. In Section II, we introduce a drone-based beamforming testbed and our experimental setup. We conduct propagation and beamforming experiments, evaluating the results in one LOS location in Section III, and two NLOS areas in Section IV. Finally, we discuss related work in Section V and conclude in Section VI.

II. BACKGROUND AND EXPERIMENTAL SETUP

In this section, we discuss the path loss models used in characterizing the drone-to-ground propagation channel over multiple frequency bands. In addition, we introduce the drone-based beamforming testbed used in the experimentation and the IEEE 802.11-like signaling used for channel feedback.

A. IEEE 802.11-Based Frame Structure

Orthogonal frequency division modulation (OFDM) systems have been widely deployed in wireless networks, including multiple generations of cellular and WiFi standards. In this work, we first use the wideband OFDM signals for air-to-ground channel propagation characterization with one transmitting antenna and IEEE 802.11 PHY frames. We implement an OFDM scheme with 64 subcarriers operating at 20-MHz bandwidth and a cyclic prefix (CP) interval of 0.25. The frame structure consists of a preamble, header, and data as specified in the standard. The data length used for these experiments is 256 bytes. Additionally, we propose an IEEE 802.11-like RTS/CTS scheme with the channel feedback required for beamforming using two transmitting antennas (see Fig. 2(a) and further discussion below). Other parameters are set as suggested in IEEE 802.11 standard and shown in Table I.

TABLE I
IEEE 802.11 BASED FRAME PARAMETERS

Parameters	Value
Central Frequencies	900 MHz, 1800 MHz, and 5 GHz
Modulation Schemes	QPSK
Total Subcarriers	52
Occupied Subcarriers	48
Pilot Subcarriers	4
FFT size	64
CP Interval	0.25

B. Path Loss Model

From the received power of the SISO measurements, we derive the relative path loss (dB) from the signal reception difference between the receiver location and the 10 m reference distance. Then, the absolute path loss model is calculated by adjusting relative path loss based on the referenced free space path loss at 10 m. The absolute path loss model is given by [13], [16]:

$$PL(d) = 20log_{10}(\frac{4\pi d_0 f}{c}) + \overline{PL}(d, d_0) + X_s \quad (1)$$

Here, $PL(d)$ is the absolute path loss (abbreviated as path loss) for a drone-receiver separation distance d. $\overline{PL}(d, d_0)$ is
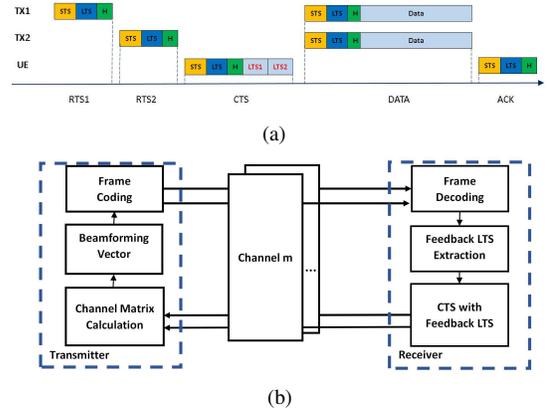
Fig. 2. Drone-based beamforming system design: (a) Beamforming Timeline (b) Transmission Diagram.

the relative path Loss from the receiver at d to the reference distance d_0. The term $20log_{10}(\frac{4\pi d_0 f}{c})$ corresponds to the path loss at d_0, where f denotes the central frequency and c represents the speed of light. X_s represents the shadow-fading parameter that follows a normal distribution with zero-mean and standard deviation σ. In this work, we first measure the signal strength at a fixed reference distance of 10 m and then calculate the relative path loss for each measurement position. For each carrier frequency and drone altitude, the path loss scatters can be plotted by adding the relative path Loss on the reference path loss.

C. Channel Feedback and Beamforming Mechanism

We implement a USRP-based SDR platform by developing a physical (PHY) and media access control (MAC) design that implements IEEE 802.11 based frames, as shown in Fig. 2(a).

We design a complete real-time OFDM beamforming system with flow control, synchronization, signal processing, and performance analysis functionalities by means of GNU Radio with out-of-tree modules. Consider a typical beamforming system in the frequency domain with M transmit antennas, one single receive antenna, and K subcarriers. At the kth subcarrier, the same copy of signal symbol $s(k)$ ($E\left[|s|^2\right] = 1$) is coded by the beamformer prior to being sent to the receiver from the mth transmit antenna. For the purpose of eliminating inter-symbol interference (ISI) and modeling a frequency-selective multipath channel as a flat-fading channel, the CP is added at each OFDM symbol. We represent $h_m(k)$ as the complex channel information obtained in the path from the mth transmit antenna to the single receive antenna at the kth subcarrier. The length of one OFDM data frame is assumed to contain a fixed number of L OFDM symbols. The preamble has two OFDM symbols with known training data. Then, the received signal at the kth subcarrier and lth OFDM symbol interval ($l = 1, ..., L$) can be written as [17]:

$$r_{k,l} = \sum_{m=1}^{M} h_m(k)w_m(k)s(k,l) + n(k,l) \quad (2)$$

Here, $w_m(k)$ represents the beamforming vector at the kth subcarrier, and $n(k,l)$ denotes the additive noise. Usually, in

theoretical studies, $h_m(k)$ is assumed to be constant within one packet and changes independently from other packets. A short packet length will lead to excessive header overhead and resulting low throughput. Conversely, a long packet length could cause relatively high BER due to outdated channel information. Hence, we experimentally examine these independence assumptions and the implication of the packet length for drone-based systems.

For beamforming at the transmitter, we choose conjugate beamforming due to its simplicity and efficiency [5], [13], [16], represented as:

$$w_m(k) = \frac{\tilde{h}_m(k)^*}{\|\tilde{h}_m(k)\|} \qquad (3)$$

Here, $()^*$ is the conjugate transpose operation, and $\tilde{h}_m(k)$ is the estimated channel information based on training symbols.

In order to efficiently achieve beamforming, the downlink channel state information (CSI) needs to be sent back from the receiver to the transmitter. For channel feedback, we use the approach proposed by [19], [20], which greatly expedites the feedback process and reduces the power consumption compared with current feedback approaches. While Shannon's capacity formula has widely been used to map the SNR to the ideal capacity [21], in current deployed networks, the throughput strictly depends on the control overhead of the handshake mechanism and successful decoding of the received frames. In this work, we derive the throughput by recording the values of BER, number of successfully decoded packets (N_s), and total transmission time (T) at each experimental position, given by the following equation:

$$Throughput = \frac{256 * 8 * N_s * (1 - BER)}{T} \qquad (4)$$

D. Hardware Setup and Experimental Calibration

The complete testbed for measurement experimentation includes the mounted SDR platform on an off-the-shelf drone and the IEEE 802.11-like framework implementation, as shown in 3. First, we have used a ROBO 3D printer to design and print secure mounts so as to fix the USRP E312 and two omni-directional vertical antennae on a DJI Matrice 100. The antenna mounts guarantee a 10-cm separation between two antennae, allowing little correlation between two streaming channels and permitting experimental repeatability. We mount two dual-band VERT900 omni-directional antennae for carrier frequencies of 900 MHz and 1800 MHz, and two VERT2450 antennae for a carrier frequency of 5 GHz. Both antenna types provide an isotropic gain of 3 dBi. Then, we have designed and implemented PHY and MAC layers that employ the IEEE 802.11-like signaling using GNU Radio [22], as shown in Fig. 2(a). During the experiments, The receiver is mounted on a tripod at a 1-m height. The received signals are processed by software blocks, and the outcomes are recorded by a laptop. We also develop shell scripts to allow the USRP to operate in an automated fashion after beginning experimentation. During the experiments, we move the receiver within a radius of five times the wavelength to average out fast-fading effects. For each test case, we complete at least 10000 frame transmissions
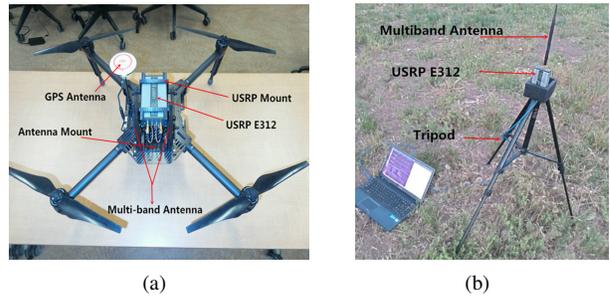
Fig. 3. Equipment settings for experiments. (a) USRP mounted on a drone (b) Receiver mounted on a tripod.

to obtain experimental reliability. In-lab calibration of USRP transmission power is performed by directly connecting the Rohde & Schwarz FSH8 SA to the USRP and adjusting the USRP configurations to normalize the power on all frequency bands. We fix the total transmission power to be 2 dBm in all antenna configurations (one antenna and two antenna schemes) by aligning the transmission power at each RF chain.

E. Experimental Procedures

We first perform in-field experiments in a Line-of-Sight (LOS) area. We investigate how wideband signals attenuate at drone altitudes with one transmit antenna, including ground, 10 m, 20 m, and 30 m, and various transmitter-receiver horizontal distances, ranging from 10 to 100 m with 10-m granularity. The dominant propagation parameters (path loss and shadowing standard deviation) are extracted and analyzed. Our experiments are conducted over three carrier frequencies: 900 MHz, 1800 MHz, and 5 GHz. Furthermore, we evaluate the performance of the beamforming with two transmit antennas by evaluating the decoding and demodulating received packets (*e.g.*, BER and successfully decoded packets). We also provide quantitative analysis on performance improvements over the IEEE 802.11 SISO scenario without beamforming. Considering many real applications are Non-Line-of-Sight (NLOS), we additionally characterize the air-to-ground channel and beamforming performance in two distinct NLOS areas: a densely-treed environment and a brush environment.

III. IN-FIELD LOS EXPERIMENTS

In this section, we perform in-field LOS measurements to characterize the air-to-ground propagation channels in terms of their propagation characteristics and evaluate the system-level performance of beamforming in such channels. In all experiments, the transmitter and receiver have an unobstructed path as depicted in Fig. 4.

Fig. 4. Physical location of in-field LOS measurements

TABLE II
ESTIMATED SHADOWING PARAMETERS (dB) UNDER VARIOUS SCENARIOS

Frequency	900 MHz				1800 MHz				5 GHz			
Drone Altitude	Ground	10 m	20 m	30 m	Ground	10 m	20 m	30 m	Ground	10 m	20 m	30 m
LOS	3.81	4.47	5.34	6.12	3.22	3.56	4.13	5.25	1.45	1.30	2.21	2.34
Tree NLOS	3.78	4.66	5.79	6.32	3.69	4.30	4.52	5.05	3.55	3.24	4.79	4.73
Brush NLOS	4.28	4.91	5.98	6.57	3.64	4.42	4.76	5.22	3.71	3.73	4.85	5.01
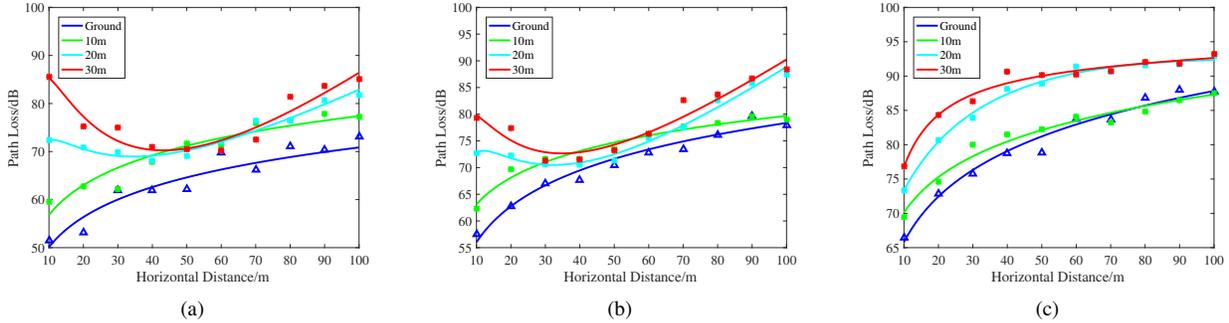
Fig. 5. Drone-to-Ground Path Loss Model in LOS Scenarios: (a) 900 MHz (b) 1800 MHz (c) 5 GHz;

A. Wideband-Based Drone-to-Ground Channel Evaluation

In order to evaluate the drone-to-ground channel, we conduct downlink wideband experiments as a function of variable horizontal distances, drone hovering altitudes, and carrier frequencies. Based on the signal level at the receiver, we can calculate the path loss and shadowing standard deviation. Fig. 5(a)(b)(c) present the path loss of the three frequency bands after linearly fitting the mean values of path loss at each horizontal distance and transmitter altitude. For carrier frequencies of 900 MHz and 1800 MHz, the signal reception seems to follow the expected pattern when the drone is on the ground and at 10-m altitude: the path loss increases as the distance increases at 10-m altitude. However, it is interesting to observe that the path loss decreases with distance at the shorter distances, and then increases from the minimum value at greater distances and at the higher altitudes. For example, 1800 MHz has a minimum value of 70.4 dB at the distance of 40 m when the drone altitude is 20 m, and then the path Loss value increases as the distance increases. This is due to the metal body of the drone that blocks the radio transmission at higher altitude and shorter horizontal distances and the omni-directional antenna pattern that better radiates at greater distances due to less obstruction. However, the path loss only increases at 5 GHz band. One reason might be the large path loss experienced at higher frequency causing clipping beyond the sensitivity level of the receiver at larger horizontal distances. This impact is equal to the radio blockage introduced by drone body at shorter horizontal distance. The fact that the path loss curve at 5 GHz at ground presents a continually increasing slope than that at higher altitude is explained by the high levels of energy dissipation in the ground at that frequency band. Additionally, the shadowing standard deviation increases as the altitude increases, as shown in Table II. In addition to the blocking problem noted, the increase in shadowing at greater altitude could also be due to the increasing impact of the wind at altitudes above the tree heights. Our evaluation reveals that higher frequency band (5 GHz) has relatively lower shadowing effects than lower frequency bands (900 and 1800 MHz) in LOS scenarios.

B. Beamforming-Based Link Performance Analysis

We now move to understanding the link performance of beamformed (2×1) transmissions that are housed on a drone using the aforementioned experimentation setup in a LOS environment. We compare the link budget of the beamforming framework proposed in this work and the conventional IEEE 802.11 scheme, at three drone altitudes (10 m, 20 m, and 30 m) at a transmitter-receiver separation distance ranging from 10 to 100 meters with 20 meter linear granularity. Table III shows the throughput results of both schemes at distances of 10 m and 50 m.[1] We observe that the highest air-to-ground throughput gains occur at the shortest distance (10 m), where beamforming provides improvements over SISO of up to 47.3%, 73.6%, and 22.7%, at drone altitudes of 30 m, 20 m, and 10 m, respectively, from lowest to highest carrier frequency. Furthermore, as distance increases, there is a significant decrease in gains at 900 MHz and 1800 MHz. When the distance is beyond 60 m, throughput for both beamforming and SISO schemes reduce to nearly zero. This is explained by the large path loss experienced at 5 GHz that causes clipping beyond the sensitivity level of the receiver as compared to the shorter distances. We conclude that beamforming results in significant throughput gain at shorter distances (10 to 50 meters) as opposed to more distant distances (60 to 100 meters).

IV. IN-FIELD NLOS EXPERIMENTS

In this section, we discuss the NLOS experiments to investigate drone-to-ground channels and throughput performance using SISO and beamformed transmissions. The NLOS scenarios include a densely-treed environment and brush environment, as shown in Fig. 7. At the time of the experiments, the pine trees in the tree environment had little foliage along the direct path from sender to receiver but have large trunks that

---

[1]Due to space limitations, we have included a condensed table of our results. However, the complete set of results at horizontal distances of 10 to 100 meters can be found at: https://goo.gl/6C7Y2g

TABLE III
ESTIMATED THROUGHPUT (MBPS) UNDER VARIOUS SCENARIOS

Scenarios		Frequency h / d_h	900 MHz				1800 MHz				5 GHz			
			Ground	10 m	20 m	30 m	Ground	10 m	20 m	30 m	Ground	10 m	20 m	30 m
LOS	Beamforming	10 m	37.64	34.87	27.58	12.59	28.73	26.58	24.87	16.39	26.81	24.73	21.59	14.58
		50 m	26.70	26.19	24.70	22.55	20.19	16.01	17.54	16.53	15.42	14.55	5.78	5.15
	SISO	10 m	23.37	20.19	16.85	8.06	21.24	18.17	9.60	7.87	11.72	12.80	11.28	10.33
		50 m	16.49	13.33	14.99	13.82	11.96	9.99	9.49	10.06	7.22	6.15	2.84	2.22
	Gain	10 m	0.386	0.339	0.375	0.473	0.318	0.288	0.736	0.348	0.260	0.227	0.187	0.155
		50 m	0.294	0.302	0.251	0.227	0.242	0.251	0.298	0.188	0.120	0.133	0.073	0.023
Tree NLOS	Beamforming	10 m	30.59	27.72	23.23	12.64	25.48	22.16	16.06	12.75	14.82	15.49	16.31	13.13
		50 m	20.55	16.57	18.93	15.04	14.50	11.43	11.31	10.55	9.65	7.47	3.82	2.75
	SISO	10 m	23.37	20.19	16.85	8.06	21.24	18.17	9.60	7.87	11.72	12.80	11.28	10.33
		50 m	16.49	13.33	14.99	13.82	11.96	9.99	9.49	10.06	7.22	6.15	2.84	2.22
	Gain	10 m	0.309	0.373	0.379	0.569	0.199	0.221	0.672	0.619	0.265	0.210	0.446	0.271
		50 m	0.246	0.242	0.263	0.088	0.213	0.144	0.192	0.0490	0.336	0.216	0.344	0.239
Brush NLOS	Beamforming	10 m	25.53	22.92	18.85	10.41	26.82	24.97	15.09	12.24	23.66	22.08	15.02	13.39
		50 m	18.41	13.15	16.13	8.58	16.27	13.99	13.25	10.77	10.03	5.32	3.38	3.91
	SISO	10 m	21.21	18.82	15.41	6.49	21.91	19.06	12.38	10.61	19.24	17.74	11.11	9.46
		50 m	13.53	10.63	11.07	7.38	11.98	10.94	10.60	8.62	7.48	4.19	1.81	3.14
	Gain	10 m	0.204	0.218	0.224	0.604	0.199	0.219	0.672	0.619	0.230	0.245	0.351	0.416
		50 m	0.361	0.237	0.458	0.163	0.213	0.144	0.192	0.049	0.341	0.271	0.869	0.244
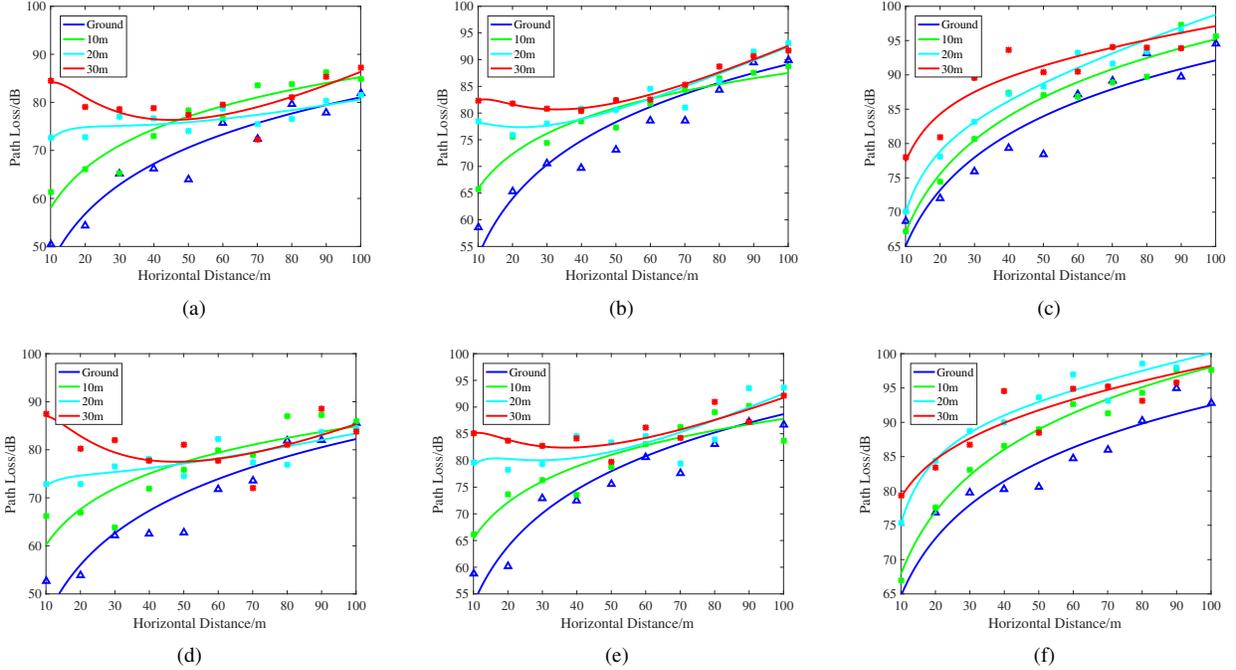
Fig. 6. Drone-to-Ground Path Loss Model in Tree NLOS Scenarios: (a) 900 MHz (b) 1800 MHz (c) 5 GHz; Drone-to-Ground Path Loss Model in Brush NLOS Scenarios.

may have obstructed transmissions. In contrast, the shrubbery in the brush environment had mature foliage but the branches of wood were relatively small (less than 2 cm in diameter).
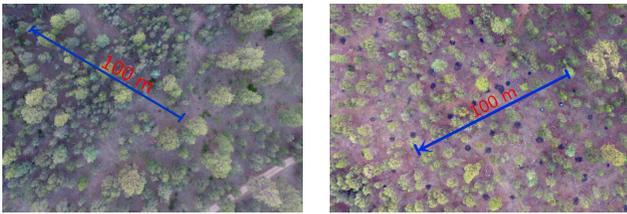
(a) Tree NLOS Area (b) Brush NLOS Area
Fig. 7. Spatial Depiction of NLOS Measurements.

A. Wideband-Based Drone-to-Ground Channel Evaluation

We use the experimental setup as discussed in Section II. As before, we linearly fit the measured values as a function of horizontal distance and drone altitude and show the results in Fig. 6. We observe that the NLOS channels present greater diversity in path loss than the LOS scenario, and the path loss tends to be larger at both shorter and farther distances. The minimum path loss at a middle horizontal distance effect previously observed in the LOS environment is still present with the NLOS environments but less dominant. This is likely due to the large impact introduced by the obstructions introduced in the more complex NLOS environments that cause higher levels of reflection, reducing the impact of the drone body blocking the transmission. Table II provides the shadowing standard deviation σ for each frequency band, which shows that these NLOS environments have greater than double the shadowing effect than the LOS environment. Furthermore, we detect a significant increase in shadowing standard deviation at 5 GHz in a range of 2 to 2.6 dB. In comparing the two NLOS environments, the brush scenario results in a higher shadowing standard deviations than the tree scenario by an average 0.27 dB. Our evaluation also reveals that the shadowing standard deviation increases as the drone altitude increases.

B. Beamforming-Based Link Performance Analysis

We now quantify the throughput improvement of beamforming compared with SISO transmissions in the same NLOS scenarios. Table III shows the SISO and beamforming throughput under different drone altitudes at 10 m and 50 m horizontal distances in Tree NLOS and Brush NLOS areas.[1] We observe that the drone-to-ground gains are more pronounced at greater horizontal distances (80 to 100 meters), especially in the brush area. In particular, beamforming provides improvements up to 90.3% and 83.1%, at drone altitudes of 30 m in the tree area, and 119.4% and 120.1% at drone altitudes of 30 m and 10 m in brush area at 900 MHz and 1800 MHz, respectively. We also find that the brush environment presents more outcomes of lower throughput than treed environment for all frequency bands, which is likely due to the much denser foliage distribution and higher signal absorption in the brush area. Furthermore, 5 GHz transmissions are more susceptible to NLOS environments than LOS since the throughputs for both schemes drop to almost zero at shorter distances (40 m). However, higher performance improvements can be found at 5 GHz in NLOS areas. For instance, beamforming at 50 m horizontal distances and 20 m drone attitude provides a gain of up to 86.9% in the brush environment.

V. RELATED WORK

The majority of the work on radio propagation for drone-to-ground channels has predominantly concentrated on simulation works without providing in-field experimental validation of simulation-based assumptions versus real geographical features and conditions [6]–[12]. For example, a channel fading model was proposed to predict the air-to-ground path loss in urban environments [6]. Simulations have also been conducted to investigate the impact of environmental attenuation on air-to-ground channels in the context of a High Altitude Platform (HAP) [7]. Other works have sought to maximize the radio coverage by optimizing the UAV position in urban environments [8]. System-level simulations also utilized path loss models to evaluate the performance of LTE and WiFi [9]. In-field experimentation has explored air-to-ground propagation to understand path loss and link performance [3], [13]–[15]. However, most of these works focus on a specific environment type at a particular frequency band without varying the drone altitude or evaluating the effectiveness of multi-antenna beamforming systems in overcoming range and connectivity issues. In contrast, we build a drone-based beamforming system using an IEEE 802.11-like signaling mechanism and characterize the drone-to-ground channels over multiple frequency bands with diverse propagation environments.

VI. CONCLUSION

In this work, we performed an in-field measurement study to characterize the drone-to-ground channels a function of distance, frequency, and drone altitude in practical LOS and NLOS scenarios across multiple frequency bands, including cellular (900 MHz and 1800 MHz), and WiFi (5 GHz) frequency bands. We presented a performance analysis of air-to-ground channels and the performance of beamforming therein with a channel feedback scheme based on IEEE 802.11-like signaling across the MAC and PHY layers. We have shown the drone-based beamforming system can boost throughput over the conventional SISO scheme at shorter distances in a LOS scenario and more distant distances in NLOS scenarios. We believe that these measurements and results will have impact on the future design of drone-based beamforming frameworks over a wide range of critical frequency bands at transmitter distances typical for WiFi and cellular systems.

REFERENCES

[1] G. V. Hoy, and B. Wang, "Forecast: Personal and Commercial Drones, Worldwide, 2016," *Gartner*, 2016.

[2] M. Erdelj, E. Natalizio, K. R. Chowdhury, and I. F. Akyildi, "Help from the Sky: Leveraging UAVs for Disaster Management," *IEEE Pervasive Computing*, 2017.

[3] Y. Gu, M. Zhou, S. Fu and Y. Wan, "Airborne WiFi networks through directional antennae: An experimental study," in *IEEE WCNC*, 2015.

[4] Y. Zeng, R. Zhang, and T. J. Lim, "Wireless communications with unmanned aerial vehicles: opportunities and challenges," in *IEEE Communications Magazine*, 2016.

[5] Y. Shi, J. Wensowitch, E. Johnson, and J. Camp. "A Measurement Study of User-Induced Propagation Effects for UHF Frequency Bands," in *2017 14th SECON*, June 2017.

[6] A. Al-Hourani, S. Kandeepan, and A. Jamalipour, "Modeling air-to-ground path loss for low altitude platforms in urban environments," in *IEEE GLOBECOM*, 2014.

[7] Y. Zheng, Y. Wang, and F. Meng, "Modeling and Simulation of Pathloss and Fading for Air-Ground Link of HAPs within a Network Simulator," *IEEE CyberC*, pp. 2013.

[8] E. Kalantari, H. Yanikomeroglu, A. Yongacoglu, "On the Number and 3D Placement of Drone Base Stations in Wireless Cellular Networks," in *IEEE VTC*, 2016.

[9] S. Chandrasekharan, A. Al-Hourani, K. Gomez, S. Kandeepan R. Evans, L. Reynaud, and S. Scalise, "Performance Evaluation of LTE and WiFi Technologies in Aerial Networks," in *IEEE GLOBECOM*, 2016.

[10] S. M. Gulfam, S. J. Nawaz, A. Ahmed and M. N. Patwary, "Analysis on multipath shape factors of air-to-ground radio communication channels," in *IEEE WTS*, 2016.

[11] M. Wentz and M. Stojanovic, "A MIMO Radio Channel Model for Low-Altitude Air-to-Ground Communication Systems," in *IEEE VTCFALL*, 2015.

[12] W. G. Newhall and J. H. Reed, "A geometric air-to-ground radio channel model," in *IEEE MILCOM*, 2002.

[13] D. W. Matolak and R. Sun, "Air-ground channel characterization for unmanned aircraft systems: The near-urban environment," in *IEEE MILCOM*, 2015.

[14] E. Yanmaz, R. Kuschnig and C. Bettstetter, Achieving Air-Ground Communications in 802.11 Networks with Three-Dimensional Aerial Mobility, in IEEE INFOCOM, 2013.

[15] M. Asadpour, D. Giustiniano, K. A. Hummel, and S. Heimlicher, Characterizing 802.11n Aerial Communication, in *ACM MobiHoc*, 2013.

[16] Y. Shi, "Improving the performance of RSS detection using wireless open-source platforms," in *IEEE Symposium on WMCS*, 2015

[17] T. S. Rappaport, "Wireless Communications: Principles and Practice, 2nd Ed," *Prentice Hall*, 2002.

[18] H. Yang and T. Marzetta, Performance of Conjugate and Zero-Forcing Beamforming in Large-Scale Antenna Systems, in *IEEE J. Sel. Areas Commun.*, 2013.

[19] Y. Ma, G. Zhou and S. Lin, "EliMO: Eliminating Channel Feedback from MIMO," in *IEEE SMARTCOMP*, 2017.

[20] D. Love and R. W. Heath Jr., Limited feedback precoding for spatial multiplexing systems, in *IEEE GLOBECOM*, 2013

[21] Y. Du, E. Aryafar, P. Cui, J. Camp and M. Chiang, "SAMU: Design and implementation of selectivity-aware MU-MIMO for wideband WiFi," in *IEEE SECON*, 2015.

[22] "The Main Page of GNU Radio," Available: https://wiki.gnuradio.org/index.php/Main_Page/